ACS APPLIED MATERIALS & INTERFACES

Research Article

www.acsami.org

Sequential Growth of Zinc Oxide Nanorod Arrays at Room Temperature via a Corrosion Process: Application in Visible Light Photocatalysis

Danish Iqbal,[†] Aleksander Kostka,[†] Asif Bashir,[†] Adnan Sarfraz,[†] Ying Chen,[†,‡,§] Andreas D. Wieck,[¶] and Andreas Erbe*[,‡]

[†]Center for Electrochemical Sciences (CES), Ruhr-Universität Bochum, 44801 Bochum, Germany

[‡]Max-Planck-Institut für Eisenforschung GmbH, Max-Planck-Str. 1, 40237 Düsseldorf, Germany

[¶]Chair for Applied Solid State Physics, Ruhr-Universität Bochum, 44801 Bochum, Germany

ABSTRACT: Many photocatalyst systems catalyze chemical reactions under ultraviolet (UV) illumination, because of its high photon energies. Activating inexpensive, widely available materials as photocatalyst using the intense visible part of the solar spectrum is more challenging. Here, nanorod arrays of the wide-band-gap semiconductor zinc oxide have been shown to act as photocatalysts for the aerobic photo-oxidation of organic dye Methyl Orange under illumination with red light, which is normally accessible only to narrow-band semiconductors. The homogeneous, 800−1000-nm-thick ZnO nanorod arrays show substantial light absorption (absorbances >1) throughout the visible spectral range. This absorption is caused by defect levels inside the band gap. Multiple scattering processes by the rods make the nanorods appear black. The dominantly crystalline ZnO nanorod structures grow in the (0001) direction, i.e., with the *c*-axis perpendicular to the surface of polycrystalline zinc. The room-temperature preparation route relies on controlled cathodic delamination of a weakly bound polymer coating from metallic zinc, an industrially produced and cheaply available substrate. Cathodic delamination is a sequential synthesis process, because it involves the propagation of a delamination front over the base material. Consequently, arbitrarily large sample surfaces can be nanostructured using this approach.

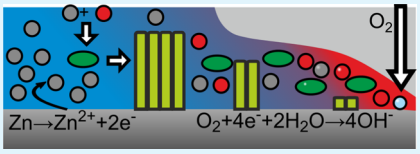

KEYWORDS: *photocatalysis, visible light, zinc oxide nanorods, corrosion, cathodic delamination*

1. INTRODUCTION

Among the big challenges in semiconductor photocatalysis is tuning the bandgap, defect levels, and morphology of the catalyst for efficient use of a large part of the visible spectrum—in particular, the red fraction of light—to catalyze chemical reactions.[1−3] So far, TiO_2 has been the most popular material of study as photocatalysts, e.g. in different nanostructures.[4−6] A particular important application of semiconductor photocatalysis is the decomposition of organic substances in water via aerobic photo-oxidation,[7,8] a potential route to remove persistant pollutants.[1,9,10] Using ultraviolet (UV) light, large conversions in decomposition of an organic dye model pollutant have been achieved.[7]

For decomposition of organic substances, many different materials are currently being investigated, including low-cost, nontoxic ZnO.[11,12] Its band gap at UV photon energies can be modified by crystal strain.[13] While application with UV light is straightforward, more current focus is directed toward extending the operational range toward visible light. In this regard, most approaches extend the ZnO light absorption from the UV into the blue part of the visible range.[12,14,15] Alternatively, metal nanoparticles can be conjugated to ZnO.[16] Supported catalysts with large surface areas can conveniently be realized as ZnO nanorod arrays.[17] Consequently developed synthesis methods include chemical vapor deposition,[18] laser decomposition of a suitable precursor,[19] vapor−liquid−solid growth,[20,21] pulsed laser deposition,[22] a flame transport method,[23] template-based methods,[24] solvothermal techniques,[25] and solution-phase approaches.[26,27] Synthesis can be interfaces with lithographic techniques for regular patterning.[28] All aforementioned preparation techniques either require the use of sophisticated instrumentation, or elevated temperature, with nanorods growing in parallel over the sample area. Besides photocatalysis, other applications of ZnO nanorod arrays include gas sensing,[25,29] refractive index sensing,[30] water splitting,[31] antibacterial coatings,[32] and solar cells.[33,34] Interesting perspectives develop when growing ZnO nanorods on cotton fibers[32,35] or galvanized steel.[36]

ZnO is also the product of zinc corrosion. Zinc is a frequently used metal which protects a base material, such as steel, against corrosion. Protection works on the one hand by zinc taking the part of the actively dissolving metal, on the other hand by forming a protective ZnO layer.[37] Corrosion processes may also be used to synthesize nanostructured materials.[38] Here, we report a strategy for sequentially fabricating highly oriented, one-dimensional (1D) ZnO nanorod arrays over large areas on metallic zinc via cathodic delamination of a polymer coating using aqueous KCl at room

Received: July 2, 2014
Accepted: October 3, 2014
Published: October 3, 2014

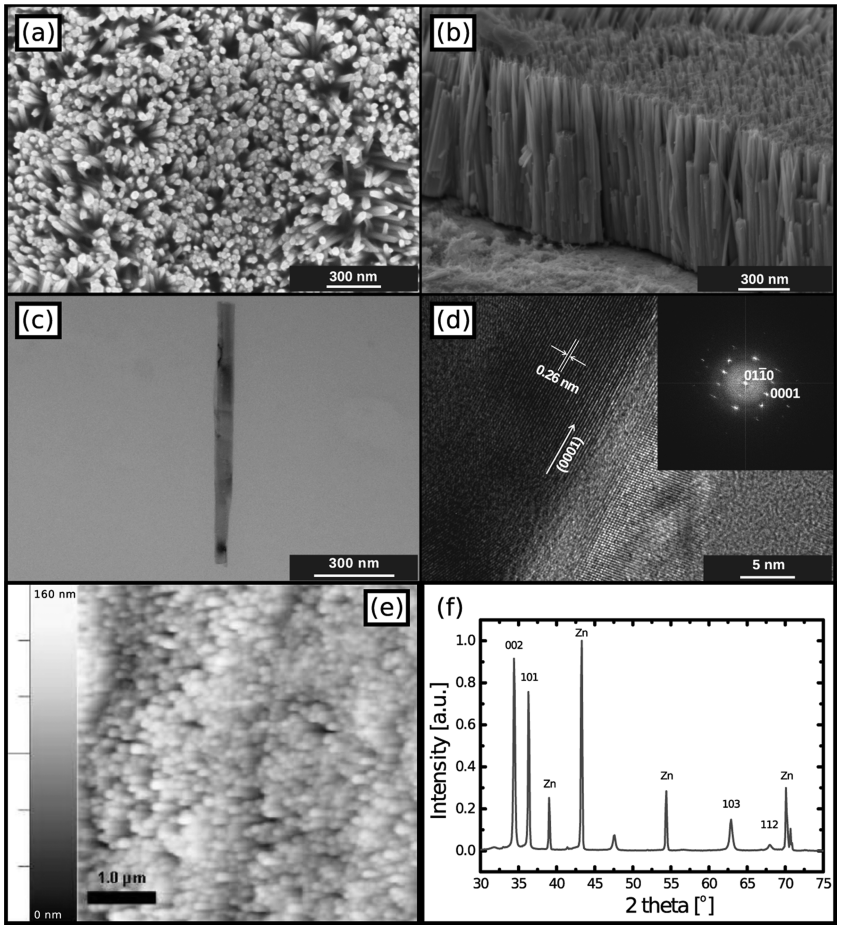

Figure 1. (a) SEM image of ZnO nanorod array grown over a zinc substrate, (b) magnified cross-sectional SEM image, (c) STEM micrograph of single nanorod, (d) HRTEM image with SAED pattern in the inset of single nanorods, (e) AFM image, and (f) XRD pattern.

temperature. Moreover, we demonstrate that the ZnO nanorods mediate the photodegradation of the organic dye Methyl Orange under illumination with red light.

2. MATERIALS AND METHODS

2.1. Materials. Poly(vinyl butyral) (PVB), absolute ethanol, Methyl Orange (MO), and KCl were obtained from Sigma–Aldrich and used as received. Zinc sheets (purity, 99.95%) with a thickness of 1.5 mm were obtained from Goodfellow (Cambridge, U.K.). Zinc sheets were initially mechanically polished using 4000 grit polishing paper and then cleaned ultrasonically in ethanol.

2.2. Synthesis of ZnO Nanostructures. Initially polished zinc sheets (1 cm × 1 cm × 1.5 mm) were spin-coated with a 5 wt % solution of PVB in ethanol, followed by drying, to obtain a 2-μm-thick polymer layer. Afterward, the coated sample was placed on a zinc base plate and a reservoir was built at the edge of the sample for electrolyte insertion with the help of a fast-drying two-component adhesive. Subsequently, a small defect was created at the edge of the coated sample with the help of a blade. The assembly was then placed into a self-made humidity chamber. In order to initiate the growth of ZnO nanorods via a tailored corrosion process, a few drops of 0.1 M (unless noted otherwise) aqueous KCl solution was added. Finally, after 6–8 h, the electrolyte was removed and substrates were washed with water and dried in an N_2 flow at room temperature.

2.3. Photocatalytic Decomposition of Methyl Orange (MO). Photocatalysis experiments were performed in a homemade continuous flow setup. Zinc foil with ZnO nanorods was placed on the bottom of a crystallization dish. Next to the foil, a magnetic stirrer was placed on the bottom of the dish. Initially, a 10^{-5} M aqueous solution of Methyl Orange (MO) (20 mL) was added into the dish, and the solution was stirred with the help of a magnetic stirrer throughout the experiment. Before starting the photocatalytic decomposition of MO, ZnO nanorod arrays were immersed in to the reaction chamber for ~30 min without illumination to establish adsorption/desorption equilibrium. Part of the MO solution was then pumped into a quartz flow cell, placed inside a UV/visible spectrometer (Perkin–Elmer, Model Lambda 900), using a peristaltic pump at a flow rate of 50 μL s^{-1}. Photocatalytic decomposition experiments were carried out with both solution and substrate at room temperature. No increase in temperature has been observed for the solution. To ensure the presence of only a specific visible wavelength of light, the sample in the glass reservoir was illuminated with a HeNe laser [Melles Griot (633 nm, 1.96 eV)] of 20 mW power output with a beam expander, yielding a power density of ~10 mW cm^{-2} at the location of the ZnO nanorods. The degradation of the dye was monitored by the ultraviolet–visible light (UV-vis) spectrometer by measuring the absorption spectra at different intervals, and evaluating the peak absorbance at 464 nm. The molar absorption coefficient of MO at 464 nm was determined to be 4×10^5 L mol^{-1} cm^{-1} from a concentration series.

2.4. Analytical Techniques. The surface morphology of ZnO nanorods was examined by scanning electron microscopy (SEM) (Zeiss/LEO, Model 1550 VP) equipped with an energy-dispersive X-ray (EDX) spectrometer (Oxford Instruments). Atomic force microscopy (AFM) images were recorded by a Digital Instruments Model Dimension 3100 AFM in tapping mode, employing Si microcantilever tips with a radius of <10 nm and a resonant frequency of ~318 kHz. Crystallographic information about the nanorods was obtained by X-ray diffraction (XRD, Bruker-AXS D8 with a Cu Kα source). X-ray photoelectron spectroscopy (XPS) (Model Quantum 2000, Physical Electronics, USA) were performed at a takeoff angle of

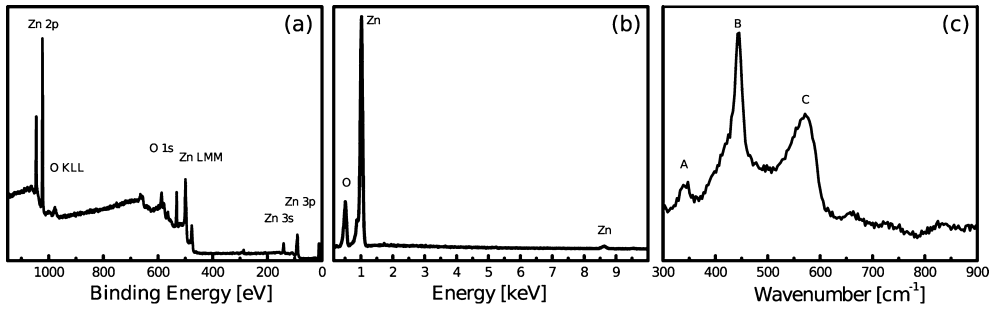

Figure 2. (a) XPS spectrum, (b) EDX spectrum, and (c) Raman spectrum of a ZnO nanorod array.

45°, with a monochromatic Al Kα source (1486.6 eV) at a pass energy of 23.5 eV. Raman spectra were recorded using a Horiba Jobin Yvon LabRAM confocal Raman microscope with excitation of a Ar^+ laser (514 nm) and a spectral acquisition time of 10 s. Photoluminescence spectra were measured using a HeCd (λ = 325 nm) laser source with an excitation power of 20 W cm^{-2}. The photoluminescence light was detected using a liquid-nitrogen-cooled InGaAs detector.

3. RESULTS AND DISCUSSION

3.1. Structure and Morphology. ZnO nanorods typically were grown for 6−8 h (maximum for 15−18 h) by coating a zinc substrate with poly(vinylbutyral) (PVB), subsequently preparing a defect in the polymer coating, and exposing the defect to a decrease of 0.1 M aqueous KCl (unless noted otherwise) at room temperature. The structure and morphology of ZnO nanorods grown over a zinc substrate were examined by scanning electron microscopy (SEM) and transmission electron microscopy (TEM) (Figure 1). The SEM micrographs demonstrate that well-ordered ZnO nanorods grow densely and uniformly over large areas (see Figures 1a and 1b). Nanorod growth was observed over the full sample, typically 1 cm^2, up to sizes of 4 cm^2, in the samples used here. Nanorod diameters range between 20 nm and 70 nm (see Figure 1a). Diameters were also verified by tapping mode atomic force microscopy (AFM; see Figure 1e). The diameter of the ZnO nanorods observed by AFM is slightly higher than that observed in SEM images. This difference results from the tip convolution, because of the high aspect ratio of ZnO nanorods.[39] The relatively flat top surfaces show that the surface is rather smooth and grown nanorods have similar lengths. The length was found to be 800−1000 nm from scanning TEM (STEM) images of single nanorods detached from the ZnO nanorods array (Figure 1c). The lattice planes of the hexagonal nanorods can be clearly seen in the high-resolution transmission electron microscopy image (HRTEM) from a single nanorod (Figure 1d), from which the selected-area diffraction (SAED) pattern (inset in Figure 1d) proves the crystalline nature with a (0001) growth direction. The crystalline nature of the formed ZnO over the complete sample area is verified by X-ray diffraction (XRD) (Figure 1f). In addition to metallic zinc peaks arising from the substrate, the sharp (002) peak of ZnO indicates the highly preferential growth of ZnO nanorods along the *c*-axis.[40]

X-ray photoelectron spectroscopy (XPS) (Figure 2a), energy-dispersive X-ray microanalysis (EDX) measurements (Figure 2b), and Raman spectroscopy (Figure 2c) confirm the purity of the resulting phase. Figure 2a shows the XPS survey spectrum obtained from surface of the nanorod arrays. Prominent peaks originating from zinc and oxygen are obvious. A small amount of carbon (~1%) is detected as a ubiquitous contaminant that is always present after sample transfer through air. In particular, the specific signatures of the PVB polymer have not been detected, which confirms the expected absence of PVB after cathodic delamination. Except for zinc, oxygen, and carbon, no other elements were detected within the sensitivity of XPS. These results are consistent with EDX, where only zinc and oxygen can be detected (Figure 2b). The semiquantitative EDX analysis yields ~55% Zn and ~45% O.

Figure 2c shows the Raman spectrum of a ZnO nanorod array. The three main peaks are marked as A, B, and C. The Raman peak at 334 cm^{-1} (peak A) is originating from a multiphonon process,[41,42] while the sharp peak at 437 cm^{-1} (peak B) corresponds to the characteristic E_2 mode of ZnO with an hexagonal Wurtzite lattice.[43,44] In addition, a broad band detected at ~578 cm^{-1} (peak C) corresponds to longitudinal optical (LO) phonons (E_1 and A_1 modes).[45] The observation of the LO phonon in the backscattering geometry used here is an indication of the presence of structural defects (see discussion given elsewhere[45−47]).

The effect of different electrolyte concentrations on the morphology of ZnO nanostructures was also investigated. In particular, by exposing the zinc substrate to a higher concentration of KCl (1 and 3 M), the diameter of 1D ZnO nanostructure was reduced from 70 nm to 10 nm. The resulting wire structures are not isolated, as in the case of lower electrolyte concentration. Instead of rods, which are observed for electrolyte concentrations below 1 M, pyramidal structures are formed, as shown in Figures 3a and 3b. An extreme case is observed when 3 M KCl is used, where thin ZnO nanowires are obtained (see Figures 3c and 3d). The different diameters observed in electrolytes with different Cl^- concentrations are attributed to the modification of growth rates on different crystal faces by Cl^- adsorption. Since different faces possess different polarities,[48,49] different susceptibility toward ion adsorption is reasonable.

The observations made in this work indicate that the ZnO nanostructures grow after the passage of a delamination front under the polymer coating, as illustrated in Figure 4.[50] The function of the polymer itself is to define a confined reaction environment, and it is not actively participating in the reaction. Because cathodic delamination represents the failure of the polymer/metal bond, there is no polymer present on the final corrosion products: the nanorod arrays. In the cathodic initial region of the delamination front, oxygen reduction leads to the formation of alkaline conditions.[50] This initial region leads to a breakage of the bond between the PVB polymer coating and the base material. After the initial part of the delamination front progressed through a certain region, the region becomes the local anode, where zinc dissolution to Zn^{2+} occurs.[50] Above a critical Zn^{2+} concentration, when the pH is >9,[51−53] zinc oxide

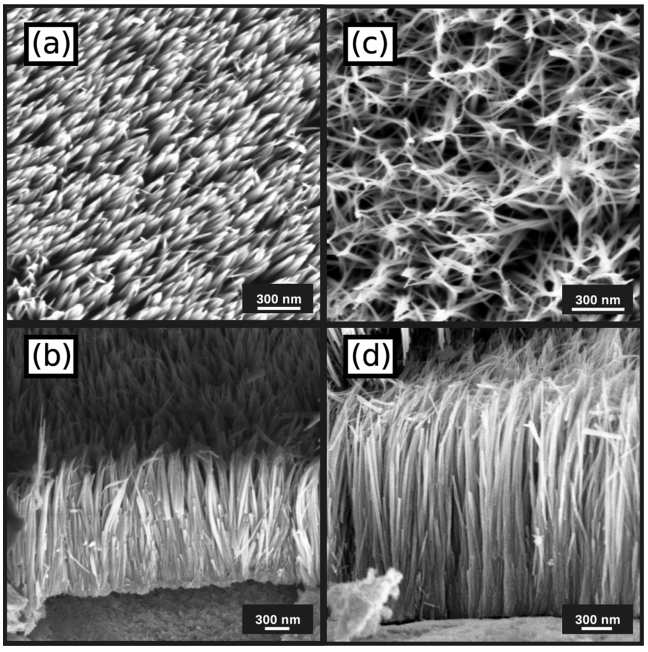

Figure 3. SEM micrographs showing the morphology of ZnO nanostructures after delamination with different electrolyte concentrations: (a, b) 1 M KCl and (c, d) 3 M KCl.

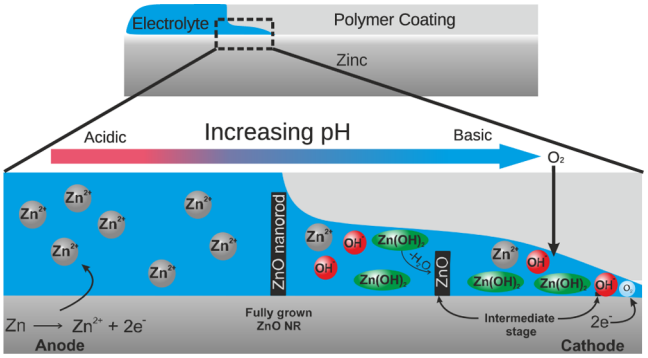

Figure 4. Schematic representation of corrosion-driven growth of ZnO nanorods arrays.

nucleates. Because of the instability of one of the fundamental surfaces of ZnO, the oxide grows in a rodlike shape, as observed here.[40,54] It is generally believed that low supersaturation levels favor growth of the 1D ZnO nanostructure.[54] A schematic view of the process of cathodic delamination and consequent corrosion product growth is shown in Figure 4. In the absence of the polymer (i.e., when homogeneous corrosion of zinc occurs), no formation of rodlike nanostructures was observed. This cathodic delamination based nanorod synthesis approach is a sequential process, as opposed to the commonly practiced synthesis approaches, in which nanorods grow in parallel over the full sample area.[18,19,22,24,26]

3.2. Light Absorption and Photocatalytic Activity. In general, electrochemically produced ZnO is known to have an electronic structure that is rather different from the electronic structure of bulk ZnO.[47,55] In thin ZnO nanorods, quantum size effects may become important and defect levels lead to an absorption of light in the visible range.[21,46,56]

Both the photoluminescence (Figure 5a) and the UV-vis reflection absorption spectrum (Figure 5b) are strongly affected by defect levels. Because luminescence is less affected by scattering than an extinction-type absorbance measurement, let us start to discuss the photoluminescence spectrum (Figure 5a) of the as-grown ZnO nanorod arrays, measured at room temperature with excitation at 325 nm (3.81 eV). The nanorods exhibit a UV emission at ∼368 nm (∼3.4 eV), which corresponds to free excitonic emission,[17] while wide visible emission band in the range of 500−700 nm (2.5−2 eV) is attributed to different structural defects in ZnO.[17,46,57−59] Emission centered at 700 nm is generally attributed to oxygen interstitials.[21,60] Emission at lower wavelengths is attributed to oxygen vacancies.[45,57] Because of the large peak width, a unique assignment of the spectrum to certain dominant defects is difficult, especially as other factors such as lattice strain cause energy shifts.[61] A recent thermodynamic analysis of energy levels of point defects shows that ZnO is unstable toward Zn vacancy formation.[62] Here, we conclude that, very likely, a combination of several types of defects contribute to the observed luminescence. A UV-vis reflection reflection absorbance spectrum of ZnO nanorods on the Zn substrate (Figure 5b) shows a strong increase in absorbance below 390 nm (3.2 eV), because of the main electronic transition in ZnO. However, in addition, a strong, structureless absorption of light is present with an absorbance of >1 throughout the visible spectral range. This strong light absorption is likely the result of a combination of multiple scattering of light in the nanorod arrays and light absorption by the nanorods.[47] The absorption is caused by defects in the ZnO crystal structure, while the rodlike morphology efficiently traps light via a multiple scattering process. Attempts to measure the scattering of light from the nanorod-covered substrates with an experimental setup as described elsewhere[63] showed scattering in off-specular direction only on the noise level. Hence, most of the extinct light intensity is really absorbed.

The absorption of visible light inspired the use of the ZnO structures in photocatalysis experiments using visible light. Previously, ZnO nanorods have been used as photocatalysts with excitation energies above the band gap (e.g., for the degradation of pollutants or bacteria).[64,65] Here, the photocatalytic degradation of MO under illumination with visible light was investigated. MO has been used in many studies as a model for organic pollutants,[1,4−7,64] although it may not be the ideal model system when investigating visible light photocatalysis, because of its strong visible absorption. Therefore, in this work, illumination with monochromatic light with a photon energy below the HOMO−LUMO separation of MO was used to rule out any other photochemical process, including an action of MO as photosensitizer. [HOMO = highest occupied molecular orbital; LUMO = lowest unoccupied molecular orbital.] After starting red illumination, UV-vis spectra of the MO solution were measured (Figure 5c) and used to calculate the concentration of MO (Figure 5d). After 6 h of illumination at 633 nm, more than 90% of MO was decomposed.

Three types of control experiments were conducted (see Figure 5d). In the first control experiment, the solution was irradiated with the laser light in the absence of nanorod arrays and no decrease in MO concentration was observed (Figure 5d, green symbols). In the second control experiment, ZnO nanorod arrays were immersed in an MO aqueous solution, and the solution's absorption spectra were recorded in the absence of illumination (Figure 5d, red symbols). In this case, a certain low decomposition was observed, but at a significantly lower rate, compared to that observed in the presence of illumination. If the light source at 633 nm is replaced by a light source at 532

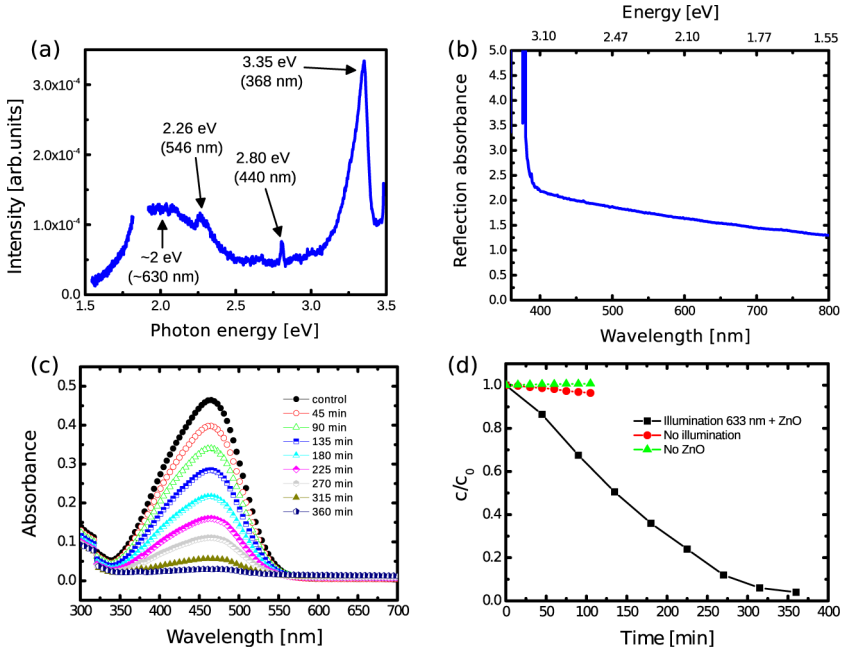

Figure 5. (a) Room-temperature photoluminescence spectrum of ZnO nanorod arrays, (b) reflection absorption spectrum of ZnO nanorod arrays (the photon energies on the top axis are rounded equivalents to the wavelengths at the corresponding label on the bottom), (c) UV-vis spectrum of Methyl Orange (MO) solution after different irradiation times, (d) molar concentration c normalized to initial molar concentration $c_0 = 10^{-5}$ mol L^{-1} of MO, as a function of time under illumination in the presence (−■−) or absence (−▲−) of ZnO nanorod arrays, as well as in the presence of ZnO nanorod arrays but without illumination (−●−).

nm (i.e., at a wavelength where the absorbance of MO is already significant), almost no decrease in MO concentration with time is observed. This observation is explained by the total absorption of light in the MO solution, resulting in a rather low intensity at the location of the ZnO nanorods. In the third type of control experiment (not shown), a zinc sheet without ZnO nanostructures (i.e., only with the native oxide) was illuminated with 633-nm light. In this case, also no photocatalytic decomposition was observed. This observation rules out the base metal itself as a catalyst.

A presumable mechanism of the observed photocatalytic activity is the binding of diradical dioxygen to the exciton generated by light absorption, and a subsequent reaction of the generated oxygen species with the organic molecules. ZnO has been shown to facilitate the generation of reactive oxygen species.[15,56] "Free electron" defects inside the ZnO are also important for the catalytic activity in methanol synthesis.[66] While the TEM images and XRD patterns confirm that crystalline ZnO is dominating in the produced nanorods, the presence of the visible photoluminescence,[57] and the LO phonon in the Raman spectrum,[47] point to a prominent presence of defects in the produced structures. Several types of defects are likely to contribute. Defect-related electronic states inside the band gap are responsible for the absorption of visible light. Since the rodlike morphology leads to strong in-plane scattering of light, even low absorption coefficients will eventually lead to photon absorption after multiple scattering events. Therefore, the observed photocatalytic activity is a consequence of a combination of morphology and defect structure in the ZnO.

While the pH stability of the ZnO nanorod arrays has not been explicitly investigated, it is strongly expected to follow the usual stability patterns of ZnO.[67] ZnO is stable at moderate pH, but dissolves in alkaline solutions under zincate formation and in strongly acidic solutions.[67] The nanorod arrays can be reused for photocatalytic experiments at least several times, with only a few percent decrease in decomposition rate. Systematic studies of the lifetime in catalytic experiments are still pending.

4. CONCLUSION

In conclusion, a tailored corrosion process based on cathodic delamination of a polymer film on metallic zinc yields dense arrays of ZnO nanorods. This room-temperature process is extraordinarily simple. It relies on a sequential process (as opposed to all preparation techniques commonly used and mentioned in the Introduction)—in this case, the passage of a delamination front. Hence, the process can easily be upscaled to large areas without the need to adjust the apparatus that is used. Furthermore, the process operates at room temperature, and no heating of any part, even to moderate temperature, is required. The resulting nanorod arrays have been shown to be able to use the red part of the visible spectrum to photocatalytically decompose MO. For this purpose, an experiment was introduced here, in which the sample system was illuminated with monochromatic light at a photon energy below the absorption of MO, ruling out contributions of photochemical processes caused by light absorption from MO. The control experiments conclusively verify that decomposition is triggered by light absorption in the ZnO nanorod arrays. The nanostructures produced by the method introduced here may potentially be used to decompose persistent pollutants. The wide availability of galvanized steel and the easy scalability of the process will enable a fabrication of the nanostructures on a square meter (m^2) scale. The nanorod synthesis scheme may also enable other (e.g., optoelectronic) applications of ZnO nanorods on large areas.

AUTHOR INFORMATION

Corresponding Author

*Tel.: +49 (0)211 6792 890. Fax: +49 (0)211 6792 218. E-mail addresses: a.erbe@mpie.de, aerbe@arcor.de.

Present Address

[§]Physik-Department E19, Technische Universität München, James-Franck-Straße 1, 85748 Garching, Germany.

Notes

The authors declare no competing financial interest.

ACKNOWLEDGMENTS

D.I. thanks the International Max Planck Research School for Surface and Interface Engineering in Advanced Materials (IMPRS-SurMat) for a scholarship. Y.C. is thankful for support from the European Union (EU) and the state of North Rhine-Westphalia in the frame of the HighTech.NRW program. We thank Prof. M. Stratmann for his continuous support and Prof. M. Muhler for helpful discussions.

REFERENCES

(1) Tong, H.; Ouyang, S.; Bi, Y.; Umezawa, N.; Oshikiri, M.; Ye, J. Nano-photocatalytic Materials: Possibilities and Challenges. *Adv. Mater.* **2012**, *24*, 229−251.

(2) Kisch, H. Semiconductor Photocatalysis—Mechanistic and Synthetic Aspects. *Angew. Chem., Int. Ed.* **2013**, *52*, 812−847.

(3) Habisreutinger, S. N.; Schmidt-Mende, L.; Stolarczyk, J. K. Photocatalytic Reduction of CO_2 on TiO_2 and Other Semiconductors. *Angew. Chem., Int. Ed.* **2013**, *52*, 7372−7408.

(4) Paramasivam, I.; Jha, H.; Liu, N.; Schmuki, P. A Review of Photocatalysis using Self-organized TiO_2 Nanotubes and Other Ordered Oxide Nanostructures. *Small* **2012**, *8*, 3073−3103.

(5) Liu, N.; Chen, X.; Zhang, J.; Schwank, J. W. A Review on TiO_2-Based Nanotubes Synthesized via Hydrothermal Method: Formation Mechanism, Structure Modification, and Photocatalytic Applications. *Catal. Today* **2014**, *225*, 34−51.

(6) Ong, W.-J.; Tan, L.-L.; Chai, S.-P.; Yong, S.-T.; Mohamed, A. R. Facet-Dependent Photocatalytic Properties of TiO_2-Based Composites for Energy Conversion and Environmental Remediation. *ChemSusChem* **2014**, *7*, 690−719.

(7) Guo, W.; Zhang, F.; Lin, C.; Wang, Z. L. Direct Growth of TiO_2 Nanosheet Arrays on Carbon Fibers for Highly Efficient Photocatalytic Degradation of Methyl Orange. *Adv. Mater.* **2012**, *24*, 4761−4764.

(8) Yang, T.-H.; Huang, L.-D.; Harn, Y.-W.; Lin, C.-C.; Chang, J.-K.; Wu, C.-I.; Wu, J.-M. High Density Unaggregated Au Nanoparticles on ZnO Nanorod Arrays Function as Efficient and Recyclable Photocatalysts for Environmental Purification. *Small* **2013**, *9*, 3169−3182.

(9) Lyu, J.; Zhu, L.; Burda, C. Considerations to Improve Adsorption and Photocatalysis of Low Concentration Air Pollutants on TiO_2. *Catal. Today* **2014**, *225*, 24−33.

(10) Wang, M.; Ioccozia, J.; Sun, L.; Lin, C.; Lin, Z. Inorganic-Modified Semiconductor TiO_2 Nanotube Arrays for Photocatalysis. *Energy Environ. Sci.* **2014**, *7*, 2182−2202.

(11) Zhang, P.; Li, B.; Zhao, Z.; Yu, C.; Hu, C.; Wu, S.; Qiu, J. Furfural-Induced Hydrothermal Synthesis of ZnO@C Gemel Hexagonal Microrods with Enhanced Photocatalytic Activity and Stability. *ACS Appl. Mater. Interfaces* **2014**, *6*, 8560−8566.

(12) Wang, J.; Wang, Z.; Huang, B.; Ma, Y.; Liu, Y.; Qin, X.; Zhang, X.; Dai, Y. Oxygen Vacancy Induced Band-Gap Narrowing and Enhanced Visible Light Photocatalytic Activity of ZnO. *ACS Appl. Mater. Interfaces* **2012**, *4*, 4024−4030.

(13) Wei, B.; Zheng, K.; Ji, Y.; Zhang, Y.; Zhang, Z.; Han, X. Size-Dependent Bandgap Modulation of ZnO Nanowires by Tensile Strain. *Nano Lett.* **2012**, *12*, 4595−4599.

(14) Etacheri, V.; Roshan, R.; Kumar, V. Mg-Doped ZnO Nanoparticles for Efficient Sunlight-Driven Photocatalysis. *ACS Appl. Mater. Interfaces* **2012**, *4*, 2717−2725.

(15) Lipovsky, A.; Tzitrinovich, Z.; Friedmann, H.; Applerot, G.; Gedanken, A.; Lubart, R. EPR Study of Visible Light-Induced ROS Generation by Nanoparticles of ZnO. *J. Phys. Chem. C* **2009**, *113*, 15997−16001.

(16) Deng, Q.; Duan, X.; Ng, D. H. L.; Tang, H.; Yang, Y.; Kong, M.; Wu, Z.; Cai, W.; Wang, G. Ag Nanoparticle Decorated Nanoporous ZnO Microrods and Their Enhanced Photocatalytic Activities. *ACS Appl. Mater. Interfaces* **2012**, *4*, 6030−6037.

(17) Djurišić, A.; Leung, Y. H. Optical Properties of ZnO Nanostructures. *Small* **2006**, *2*, 944−961.

(18) Wu, J. J.; Liu, S. C. Catalyst-Free Growth and Characterization of ZnO Nanorods. *J. Phys. Chem. B* **2002**, *106*, 9546−9551.

(19) Hong, S.; Yeo, J.; Manorotkul, W.; Kang, H. W.; Lee, J.; Han, S.; Rho, Y.; Suh, Y. D.; Sung, H. J.; Ko, S. H. Digital Selective Growth of a ZnO Nanowire Array by Large Scale Laser Decomposition of Zinc Acetate. *Nanoscale* **2013**, *5*, 3698−3703.

(20) Yang, F.; Liu, W.-H.; Wang, X.-W.; Zheng, J.; Shi, R.-Y.; Zhao, H.; Yang, H.-Q. Controllable Low Temperature Vapor-Solid Growth and Hexagonal Disk Enhanced Field Emission Property of ZnO Nanorod Arrays and Hexagonal Nanodisk Networks. *ACS Appl. Mater. Interfaces* **2012**, *4*, 3852−3859.

(21) Willander, M.; Nur, O.; Bano, N.; Sultana, K. Zinc Oxide Nanorod-Based Heterostructures on Solid and Soft Substrates for White-Light-Emitting Diode Applications. *New J. Phys.* **2009**, *11*, 125020.

(22) Choi, J. H.; Tabata, H.; Kawai, T. Initial Preferred Growth in Zinc Oxide Thin Films on Si and Amorphous Substrates by a Pulsed Laser Deposition. *J. Cryst. Growth* **2001**, *226*, 493−500.

(23) Reimer, T.; Paulowicz, I.; Röder, R.; Kaps, S.; Lupan, O.; Chemnitz, S.; Benecke, W.; Ronning, C.; Adelung, R.; Mishra, Y. K. Single Step Integration of ZnO Nano- and Microneedles in Si Trenches by Novel Flame Transport Approach: Whispering Gallery Modes and Photocatalytic Properties. *ACS Appl. Mater. Interfaces* **2014**, *6*, 7806−7815.

(24) Li, Y.; Meng, G. W.; Zhang, L. D.; Phillipp, F. Ordered Semiconductor ZnO Nanowire Arrays and their Photoluminescence Properties. *Appl. Phys. Lett.* **2000**, *76*, 2011−2013.

(25) Rai, P.; Kwak, W.-K.; Yu, Y.-T. Solvothermal Synthesis of ZnO Nanostructures and Their Morphology-Dependent Gas-Sensing Properties. *ACS Appl. Mater. Interfaces* **2013**, *5*, 3026−3032.

(26) Taghavi, M.; Mattoli, V.; Mazzolai, B.; Filippeschi, C.; Beccai, L. Synthesizing Tubular and Trapezoidal Shaped ZnO Nanowires by an Aqueous Solution Method. *Nanoscale* **2013**, *5*, 3505−3513.

(27) Pradel, K. C.; Wu, W.; Zhou, Y.; Wen, X.; Ding, Y.; Wang, Z. L. Piezotronic Effect in Solution-Grown *p*-Type ZnO Nanowires and Films. *Nano Lett.* **2013**, *13*, 2647−2653.

(28) Kim, S. B.; Lee, W. W.; Yi, J.; Park, W. I.; Kim, J.-S.; Nichols, W. T. Simple, Large-Scale Patterning of Hydrophobic ZnO Nanorod Arrays. *ACS Appl. Mater. Interfaces* **2012**, *4*, 3910−3915.

(29) Park, S.; An, S.; Ko, H.; Jin, C.; Lee, C. Synthesis of Nanograined ZnO Nanowires and Their Enhanced Gas Sensing Properties. *ACS Appl. Mater. Interfaces* **2012**, *4*, 3650−3656.

(30) Moirangthem, R. S.; Erbe, A. Interfacial Refractive Index Sensing Using Visible-Excited Intrinsic Zinc Oxide Photoluminescence Coupled to Whispering Gallery Modes. *Appl. Phys. Lett.* **2013**, *103*, 051108.

(31) Pan, K.; Dong, Y.; Zhou, W.; Pan, Q.; Xie, Y.; Xie, T.; Tian, G.; Wang, G. Facile Fabrication of Hierarchical TiO_2 Nanobelt/ZnO Nanorod Heterogeneous Nanostructure: An Efficient Photoanode for Water Splitting. *ACS Appl. Mater. Interfaces* **2013**, *5*, 8314−8320.

(32) Manna, J.; Begum, G.; Kumar, K. P.; Misra, S.; Rana, R. K. Enabling Antibacterial Coating via Bioinspired Mineralization of Nanostructured ZnO on Fabrics under Mild Conditions. *ACS Appl. Mater. Interfaces* **2013**, *5*, 4457−4463.

(33) Kim, H.; Jeong, H.; An, T. K.; Park, C. E.; Yong, K. Hybrid-Type Quantum-Dot Cosensitized ZnO Nanowire Solar Cell with Enhanced Visible-Light Harvesting. *ACS Appl. Mater. Interfaces* **2013**, *5*, 268−275.

(34) McCune, M.; Zhang, W.; Deng, Y. High Efficiency Dye-Sensitized Solar Cells Based on Three-Dimensional Multilayered ZnO Nanowire Arrays with Caterpillar-like Structure. *Nano Lett.* **2012**, *12*, 3656−3662.
(35) Athauda, T. J.; Hari, P.; Ozer, R. R. Tuning Physical and Optical Properties of ZnO Nanowire Arrays Grown on Cotton Fibers. *ACS Appl. Mater. Interfaces* **2013**, *5*, 6237−6246.
(36) Velazquez, B. J. M.; Baskaran, S.; Gaikwad, A. V.; Ngo-Duc, T.-T.; He, X.; Oye, M. M.; Meyyappan, M.; Rout, T. K.; Fu, J. Y.; Banerjee, S. Effective Piezoelectric Response of Substrate-Integrated ZnO Nanowire Array Devices on Galvanized Steel. *ACS Appl. Mater. Interfaces* **2013**, *5*, 10650−10657.
(37) Zhang, X. G. *Corrosion and Electrochemistry of Zinc*; Plenum Press: New York, 1996.
(38) Yu, H. D.; Zhang, Z. P.; Han, M. Y. Metal Corrosion for Nanofabrication. *Small* **2012**, *8*, 2621−2635.
(39) Park, W. I.; Yi, G.-C.; Kim, J.-W.; Park, S.-M. Schottky Nanocontacts on ZnO Nanorod Arrays. *Appl. Phys. Lett.* **2003**, *82*, 4358−4360.
(40) Vayssieres, L. Growth of Arrayed Nanorods and Nanowires of ZnO from Aqueous Solutions. *Adv. Mater.* **2003**, *15*, 464−466.
(41) Calleja, J. M.; Cardona, M. Resonant Raman-Scattering in ZnO. *Phys. Rev. B* **1977**, *16*, 3753−3761.
(42) Özgür, Ü.; Alivov, Y. I.; Liu, C.; Teke, A.; Reshchikov, M. A.; Doğan, S.; Avrutin, V.; Cho, S.-J.; Morkoç, H. A Comprehensive Review of ZnO Materials and Devices. *J. Appl. Phys.* **2005**, *98*, 041301.
(43) Damen, T. C.; Porto, S. P. S.; Tell, B. Raman Effect in Zinc Oxide. *Phys. Rev.* **1966**, *142*, 570−574.
(44) Arguello, C. A.; Rousseau, D. L.; Porto, S. P. S. First-Order Raman Effect in Wurtzite-Type Crystals. *Phys. Rev.* **1969**, *181*, 1351−1363.
(45) Tay, Y. Y.; Tan, T. T.; Liang, M. H.; Boey, F.; Li, S. Nature of Quasi-LO Phonon in ZnO. *Appl. Phys. Lett.* **2008**, *93*, 111903.
(46) Wang, M.; Zhou, Y.; Zhang, Y.; Kim, E. J.; Hahn, S. H.; Seong, S. G. Near-Infrared Photoluminescence from ZnO. *Appl. Phys. Lett.* **2012**, *100*, 101906.
(47) Chen, Y.; Schneider, P.; Liu, B.-J.; Borodin, S.; Ren, B.; Erbe, A. Electronic Structure and Morphology of Dark Oxides on Zinc Generated by Electrochemical Treatment. *Phys. Chem. Chem. Phys.* **2013**, *15*, 9812−9822.
(48) Wöll, C. The Chemistry and Physics of Zinc Oxide Surfaces. *Prog. Surf. Sci.* **2007**, *82*, 55−120.
(49) Dag, S.; Wang, S.; Wang, L.-W. Large Surface Dipole Moments in ZnO Nanorods. *Nano Lett.* **2011**, *11*, 2348−2352.
(50) Fürbeth, W.; Stratmann, M. The Delamination of Polymeric Coatings from Electrogalvanised steel—A Mechanistic Approach: Part 1: Delamination from a Defect with Intact Zinc Layer. *Corros. Sci.* **2001**, *43*, 207−227.
(51) Yamabi, S.; Imai, H. Growth Conditions for Wurtzite Zinc Oxide Films in Aqueous Solutions. *J. Mater. Chem.* **2002**, *12*, 3773−3778.
(52) Peulon, S.; Lincot, D. Mechanistic Study of Cathodic Electrodeposition of Zinc Oxide and Zinc Hydroxychloride Films from Oxygenated Aqueous Zinc Chloride Solutions. *J. Electrochem. Soc.* **1998**, *145*, 864−874.
(53) Xu, C. K.; Shin, P.; Cao, L. L.; Gao, D. Preferential Growth of Long ZnO Nanowire Array and Its Application in Dye-Sensitized Solar Cells. *J. Phys. Chem. C* **2010**, *114*, 125−129.
(54) Weintraub, B.; Zhou, Z.; Li, Y.; Deng, Y. Solution Synthesis of One-Dimensional ZnO Nanomaterials and their Applications. *Nanoscale* **2010**, *2*, 1573−1587.
(55) Zuo, J.; Erbe, A. Optical and Electronic Properties of Native Zinc Oxide Films on Polycrystalline Zn. *Phys. Chem. Chem. Phys.* **2010**, *12*, 11467−11476.
(56) Guo, M. Y.; Ng, A. M. C.; Liu, F.; Djurišić, A.; Chan, W. K.; Su, H.; Wong, K. S. Effect of Native Defects on Photocatalytic Properties of ZnO. *J. Phys. Chem. C* **2011**, *115*, 11095−11101.
(57) Vanheusden, K.; Warren, W. L.; Seager, C. H.; Tallant, D. R.; Voigt, J. A.; Gnade, B. E. Mechanisms Behind Green Photoluminescence in ZnO Phosphor Powders. *J. Appl. Phys.* **1996**, *79*, 7983−7990.
(58) Wang, J.; Liu, P.; Fu, X.; Li, Z.; Han, W.; Wang, X. Relationship between Oxygen Defects and the Photocatalytic Property of ZnO Nanocrystals in Nafion Membranes. *Langmuir* **2009**, *25*, 1218−1223.
(59) Zhao, D.; Zhang, C.; Zhang, X.; Cai, L.; Zhang, X.; Luan, P.; Zhang, Q.; Tu, M.; Wang, Y.; Zhou, W.; Li, Z.; Xie, S. Substrate-Induced Effects on the Optical Properties of Individual ZnO Nanorods with Different Diameters. *Nanoscale* **2014**, *6*, 483−491.
(60) Pierce, B. J.; Hengehold, R. L. Depth-Resolved Cathodoluminescence of Ion-Implanted Layers in Zinc Oxide. *J. Appl. Phys.* **1976**, *47*, 644−651.
(61) Xu, S.; Guo, W.; Du, S.; Loy, M. M. T.; Wang, N. Piezotronic Effects on the Optical Properties of ZnO Nanowires. *Nano Lett.* **2012**, *12*, 5802−5807.
(62) Todorova, M.; Neugebauer, J. Connecting Semiconductor Defect Chemistry with Electrochemistry: Impact of the Electrolyte on the Formation and Concentration of Point Defects in ZnO. *Surf. Sci.* **2014**, in press (DOI: 10.1016/j.susc.2014.07.023).
(63) Auinger, M.; Ebbinghaus, P.; Blümich, A.; Erbe, A. Effect of Surface Roughness on Optical Heating of Metals. *J. Europ. Opt. Soc. Rap. Public.* **2014**, *9*, 14004.
(64) Lu, F.; Cai, W. P.; Zhang, Y. G. ZnO Hierarchical Micro/Nanoarchitectures: Solvothermal Synthesis and Structurally Enhanced Photocatalytic Performance. *Adv. Funct. Mater.* **2008**, *18*, 1047−1056.
(65) Sapkota, A.; Anceno, A. J.; Baruah, S.; Shipin, O. V.; Dutta, J. Zinc Oxide Nanorod Mediated Visible Light Photoinactivation of Model Microbes in Water. *Nanotechnology* **2011**, *22*, 215703.
(66) Polarz, S.; Strunk, J.; Ischenko, V.; van den Berg, M. W. E.; Hinrichsen, O.; Muhler, M.; Driess, M. On the Role of Oxygen Defects in the Catalytic Performance of Zinc Oxide. *Angew. Chem., Int. Ed.* **2006**, *45*, 2965−2969.
(67) Pourbaix, M. *Atlas of Electrochemical Equilibria in Aqueous Solutions*; National Association of Corrosion Engineers/Centre Belge d'Etude de la Corrosion CEBELCOR: Houston, TX/Bruxelles, 1974.